Construction and Building Materials 426 (2024) 136133

Contents lists available at ScienceDirect

Construction and Building Materials

journal homepage: www.elsevier.com/locate/conbuildmat

Bond of post-tensioning strands in case of grouting defects

Daniele Ferretti *, Federico Pagliari, Beatrice Belletti

Department of Engineering and Architecture, University of Parma, Parco Area delle Scienze 181/A, Parma, 43124, Italy

ARTICLE INFO

Keywords:
Bond–slip
Post-tensioning
Tendon
Grout defect
Strand

ABSTRACT

This paper investigates the problem of bond in post-tensioning strands in the presence of grout injection defects. In particular, the paper describes a campaign of experimental pull-out tests with a single 7-wire steel strand in the centre of a galvanised sheet metal duct with no grouting defects and with 25% and 50% defects, i.e. voids in the cross-section area of the grout. The grouted length is short in order to obtain a local bond–slip relationship. This relationship has an initial branch followed by a jump descent and a subsequent growing branch in the form of a sawtooth. The experimental data are used to define a specific bond–slip relationship that takes into account the presence of defects. The results show that the obtained bond–slip law is very different from those proposed in the literature for the case of ribbed steel bars. Furthermore, the defects cause a decrease in bond stresses and a flattening of the shape of bond–slip curves.

1. Introduction

In post-tensioned reinforced concrete structures, prestressing strands are fixed by anchors and then bonded to the concrete by injection of cementitious grout. For this reason, unlike pre-tension, the problem of the bond between strands and grout is not fundamental and has been very little studied [1,2]. This is true also for tendons composed of multiple strands. However, there are some exceptional situations where the bond becomes important even in post-tensioned structures.

One such situation is the failure of an anchor due to corrosion. In this case, the strand re-enters by sliding with respect to the surrounding concrete [3,4]. The behaviour is similar to that observed when strands are cut in pre-tensioned structures [5]. Also, the break of a strand along the beam due to impact or corrosion shows similar strand re-entry [6]. The length affected by the re-entry of the strand is called the "re-anchorage length" or "secondary anchorage length" and is of particular interest in determining the area of the beam affected by the failure and in calculating the residual capacity of the beam. [3,6]. The designer of strengthening measures also needs to know the extension of the area actually prestressed. The value of the re-anchorage length depends on the bond–slip law of the system composed of strand, grout, duct, and concrete [3,4,6,7].

Another situation where the bond–slip law is important is the presence of overloads which cause the concrete to crack and the strand to slip out, increasing the crack width. In this case, the length of the strand affected by slip is usually referred to as the "flexural bond length".

In terms of bonding, the behaviour of post-tensioned strands is similar to that of pre-tensioned strands, but with some important differences. For pre-tensioned strands, three adhesion mechanisms between strand and concrete have been identified [8,9]: (a) chemical adhesion; (b) friction; (c) mechanical interlock. Chemical adhesion between steel wires of the strand and concrete vanishes for very small slips. Friction occurs between the outer surfaces of the steel wires and the concrete as they slip. Mechanical interlock, also known as lack-of-fit, is due to the helical geometry of the strand as it passes through the helical groove in the grout left by the strand in front of it. In this movement, the strand deforms and tends to rotate [10,11]. These phenomena are related to the Hoyer's effect, i.e. the expansion/contraction of the cross-section of the strand due to the increase/decrease in stress [12,13]. The behaviour of the strand is therefore quite different from that of a ribbed bar [10].

Bond failure can occur by slippage of the strand or by splitting of the surrounding concrete [14]. In the case of post-tensioned reinforcement, the rupture of concrete by splitting is generated by the duct, which in principle can slip with respect to the concrete, acting as a large-diameter ribbed bar [14]. The strand is not surrounded by concrete but by grout which is confined by the duct, which also prevents it from cracking by splitting. The mechanical properties of the grout are therefore different from those of the concrete. Furthermore, in the case of grout voids due to injection defects, the effect of duct confinement is somehow impaired [15].

The forces exerted by the ensemble consisting of strand, grout, and duct to the concrete can be thought of as bond stresses along the longitudinal axis of the strand. In this case, the adhesion mechanisms are usually described by a relationship that relates the bond stress τ to the slip s of the strand with respect to the surrounding concrete.

* Corresponding author.
E-mail addresses: daniele.ferretti@unipr.it (D. Ferretti), federico.pagliari@unipr.it (F. Pagliari), beatrice.belletti@unipr.it (B. Belletti).

https://doi.org/10.1016/j.conbuildmat.2024.136133
Received 15 January 2024; Received in revised form 10 March 2024; Accepted 2 April 2024
Available online 12 April 2024

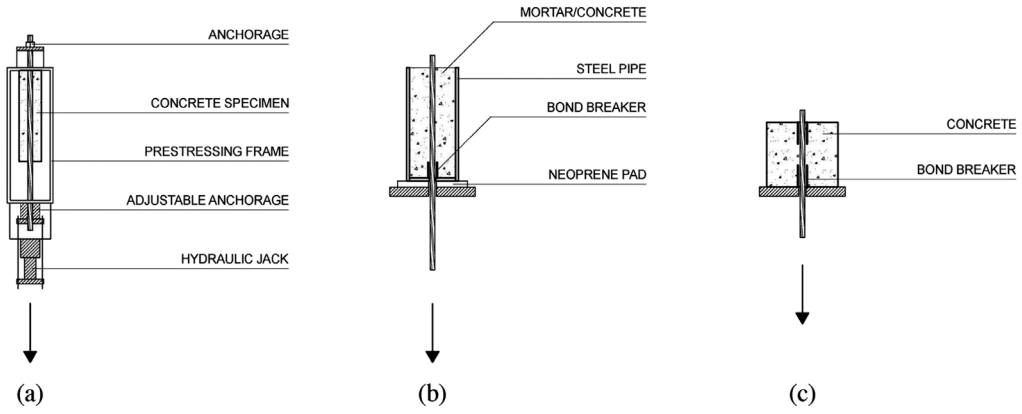

Fig. 1. Common bond test setups for strands: (a) Pull-out with pre-tensioned strand; (b) Standard Test for Strand Bond (STSB); (c) Pull-out.

Several test setups have been proposed in the literature to study adherence in pre-tensioned strands and to define the bond–slip relationship. To properly consider Hoyer's effect, some authors have proposed to perform the test with the pre-tensioned strand [16–19]. Specifically, the strand is pre-tensioned using a metal frame, then grout is injected around it. Subsequently, the pre-tensioning force is varied by activating Hoyer's effect, and finally, the bond test is performed, without removing the frame. Fig. 1a shows the test scheme. An increase in the pre-tensioning force causes the strand to shrink, detaching from the concrete and reducing bond stresses. Conversely, a reduction in force causes the strand to widen with an increase in bond stresses. For this reason, some Authors [9,20] distinguish between bond laws for the transmission length and bond laws for the flexural bond length since they have opposite Hoyer's effects. Because the test should be performed for different values of the pre-stress force, a large number of tests have to be carried out. In addition, the test is very dangerous for the operators in case of accidental breakage of the strand or pre-tensioning system. For this reason, some authors have preferred to perform the test with an untensioned strand and to correct the bond–slip relationship with an appropriate coefficient, calibrated in advance, which takes into account the Hoyer's effect [21–23]. Of these tests, the Standard Test for Strand Bond (STSB) setup is perhaps the best known [24]. The test originated to check for good strand adhesion but has also been used to calibrate the bond–slip relationship [25]. In this case, the strand, untensioned, is in the centre of a concrete cylinder (mortar is used in the original test) that is cast inside a steel tube that confines it to prevent concrete splitting cracks (Fig. 1b). The specimen rests on a layer of neoprene to allow rotations due to the helical shape of the strand.

Other authors use the classic pull-out setup for steel rebars [26], sometimes inserting stirrups into the concrete block to avoid splitting cracks (Fig. 1c). For post-tensioned strands, perhaps because of its simplicity, this is the most commonly used setup in the literature [14,27,28].

For instance, Kobrosli et al. [14,28] performed pull-out test with an unstressed strand (Fig. 1c) observing that galvanised sheet metal ducts provide better adhesion to the surrounding concrete than plastic ones. Furthermore, the authors observed better bond behaviour for circular ducts than for flat ducts. Lüthi et al. [29] came to similar conclusions. The latter authors studied also how the oil, used to protect the strand from corrosion during on-site storage, affects the bond if it is not removed before use. Laco et al. [30], using pull-out tests, observed an important bond reduction caused by oil protection of the strand.

Guo et al. [15,31] carried out pull-out test to study the effect of injection defects on the bond–slip relationship. The authors investigated four levels of defect in the cross-section of the duct. They also assumed that the defect extended over the entire bonded length (l_b = 500 mm) or a portion of it (l_b = 200 mm). Assuming that the bond stresses are constant along the bonded length, dividing the force by the strand's effective surface, the authors derived the experimental bond–slip curves. The curve has three phases: an upward branch, a downward branch, and a subsequent hardening. For major defects, the bond stresses and the slope of the hardening branch decrease. The authors proposed also a bond–slip law: the first two branches were represented with linear functions while the hardening branch with a power law.

Asp et al. [4] studied the effect of grouting defects in case of tendons composed of multiple strands. The authors, after performing some preliminary tests to evaluate the bond–slip law, studied true-size concrete elements with eccentric strands within the duct in the presence or absence of grout defects. The authors observed that a grouting defect increases the re-anchoring length.

Xiong et al. [27] performed pull-out tests to study bond in the case of retarded binder in the grout. The authors studied the difference between prismatic and cylindrical concrete specimens. The experimental bond–slip curves after the peak present an oscillatory decreasing trend. The authors proposed an analytical model for the entire curve that also accounts for the oscillations.

It should be pointed out that to compute the bond stresses τ, some authors refer conventionally to the surface area of the cylinder circumscribing the strand $\pi d_p l_b$ while others refer to the effective external surface of the strand $4\pi d_p l_b/3$, where d_p is the strand diameter.

If the duct contains several strands, only part of the surface of the strands is in contact with the grout and the bond must be modified accordingly [32]. Also Lüthi et al. [33] investigated the bond in case of multiple strands or curvature of the duct. In some cases, they also observed oscillations of the bond–slip curve after the peak.

As can be seen from this brief review of scientific publications, there is very little experimental work in the literature on bond of post-tensioned strands in the presence of grout injection defects, and the findings are sometimes contradictory. The few that exist use rather long bond lengths l_b. Bond stresses decrease along the bonded length until they nullify if the bonded length is sufficiently long. To measure a "local" bond–slip law, it is necessary to minimise the bonded length. Tepfers et al. [1] recommend a length of three to five strand diameters. This allows for virtually constant stresses along the bonded length and is not significantly affected by grouting defects and imperfections. Shorter lengths would not accurately represent the mechanical problem and could result in bond–slip laws that are widely dispersed [1].

The purpose of this paper is to extend the experimental knowledge on the bond of post-tensioned 7-wires mono-strands with galvanised duct in the presence of grout injection defects.

The following section describes the experimental campaign, which involves pull-out tests of unstressed strands using short bonded lengths l_b and two defect areas. The subsequent section presents a local bond–slip relationship, $\tau - s$, based on experimental results without defects. The last section extends this relationship to the case of defects.

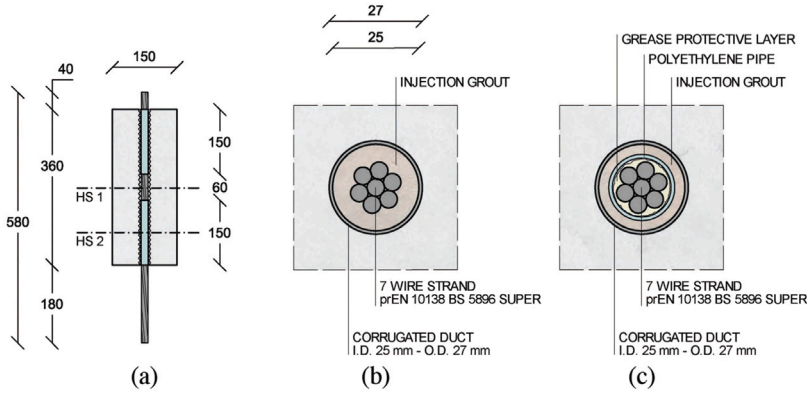

Fig. 2. Specimen geometry (dimensions in mm): (a) Longitudinal section; (b) Transversal section HS1; (c) Transversal section HS2.

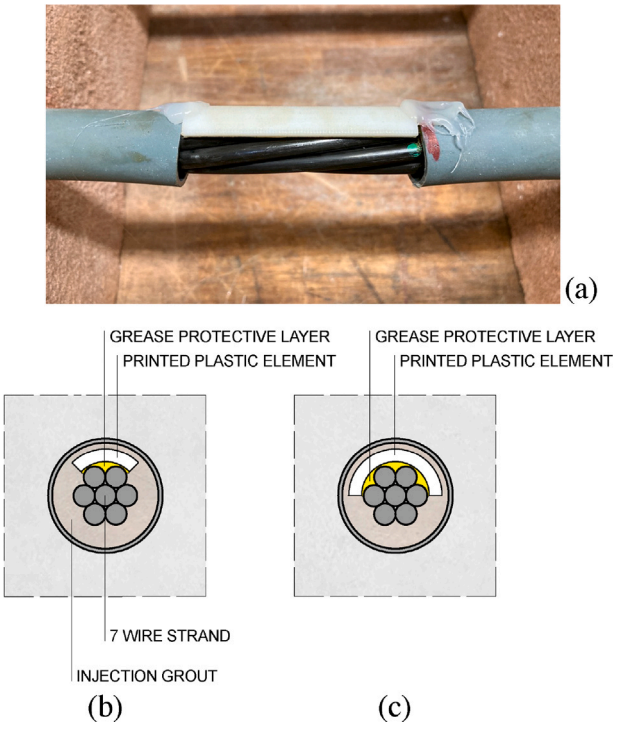

Fig. 3. Realisation of specimen defects: (a) Photo of the plastic cap and the protection pipe; (b) Cross section with defect 25%; (c) Cross section with defect 50%.

The work is preparatory to the study of the bond in the presence of injection defects and different levels of corrosion.

2. Experimental campaign

2.1. Preparation of the specimens

Pull-out tests were performed on prismatic specimens shown in Fig. 2. They consist of a concrete prism measuring 150 mm × 150 mm × 360 mm. The side 150 mm was chosen to avoid concrete splitting during the test. In particular, to prevent concrete splitting failure produced by the corrugated duct, prototypes with sides measuring 100 mm and 150 mm were tested. The 100 mm specimens cracked due to splitting, but none of the 150 mm specimens showed splitting cracks. In the centre of the prism is a 25 mm inner diameter (27 mm outer diameter) galvanised corrugated sheet metal duct of thickness approximately 0.50 mm. A 7-wire strand of 15.7 mm (0.6 in) diameter and 268 mm pitch, was placed inside the duct. Although in real cases it is possible to have the strand in contact with the duct, especially if this is curvilinear, the strand has been positioned in the centre of the duct for simplicity of testing and for repeatability and symmetry. The strand was temporarily held in the centre of the duct by two plastic rings made using 3D printing. The rings were designed with an external truncated cone shape to close the duct like a plug. Then, cementitious grout was injected at low pressure between the duct and the strand. The grout was only bonded into the 60 mm central part (approximately 4 strand diameters, Fig. 2a). In the remaining parts, the strand was protected by inserting it into a polyethylene prestressing pipe with protective grease in between (Fig. 2b). The choice of a bonded length of 4 diameters resulted in almost uniform bond stresses in the central part of the specimen [1]. The bond zone was placed in the centre of the prism to have a symmetrical specimen. This will be important in a forthcoming work where identical specimens are subject to artificial corrosion.

To simulate the presence of injection defects, with voids and missing mortar, 3D-printed plastic elements were inserted in the central part, between strand and duct (Fig. 3a). The internal surface of the plastic element was smooth to avoid interfering with the strand. The space between the strand and the plastic element was filled with prestressing grease to prevent mortar ingress. Although it was not a real void, this has allowed the adhesion in the defect area to be eliminated. Two types of defects were prepared: one with an area of 25% of the grout cross section area (Fig. 3b), and the other with an area of 50% (Fig. 3c). To ensure proper specimen preparation, prototypes were cut in half after the grout had hardened. This allowed for observation of correct grout injection, with a tolerance of 2–3 mm on the adhesion length.

A total of 18 specimens were prepared: 6 without defects, 6 with defects of 25%, and 6 with defects of 50%. The specimens were labelled with the abbreviation NC (Not Corroded), followed by the indication of the defectivity level (ND for not defected, D25 for defects of 25%, and D50 for defects of 50%).

The specimens were stored for at least 75 days in the laboratory after the injection of grout at a temperature of 20 ± 5 °C before testing.

2.2. Mechanical properties of the materials

The concrete blocks were manufactured at a prefabrication plant using a concrete made with 1000 kg of round siliceous aggregate with a maximum diameter of 14 mm, 275 kg of cement 32.5 R and 75 kg of water (water/cement ratio equal to 0.27).

To assess its mechanical strength, 4 cubes were tested according to EN 12390–3 standard [34]. The average cubic compressive strength was R_c = 39.0 (1.39) MPa, where the standard deviation is reported within parentheses. Five cylinders were tested according to EN 12390-6:2010 [35] obtaining an average Brazilian tensile strength f_t = 2.8 (0.47) MPa. All the specimens were stored in laboratory conditions and tested after 9 months, at the same time as pull-out tests.

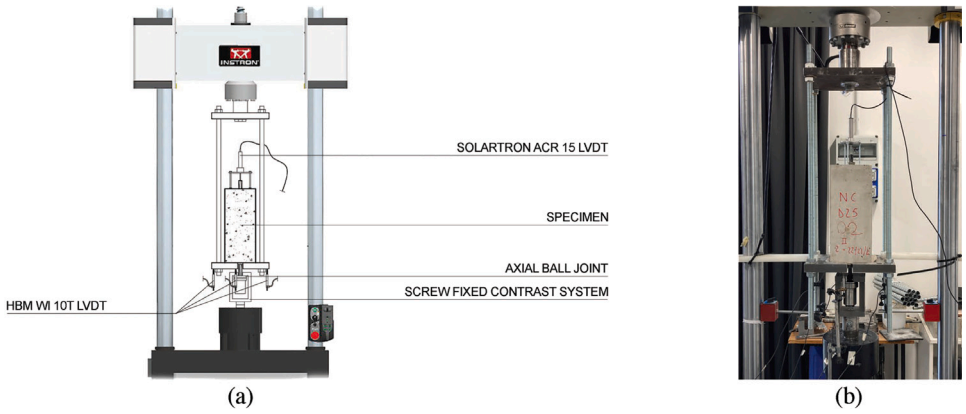

Fig. 4. Experimental setup: (a) Sketch; (b) Photography.

The grout was prepared by mixing cement, water, and superplasticiser at a ratio of 1:0.4:0.06 by weight. Flexural and compressive strength of hardened grout were measured according to EN 196-1:2005 [36] using 40 mm × 40 mm × 160 mm specimens. Bending tests were performed on a 100 mm span with a load speed of 50 ± 10 N/s; compression tests were performed on the fragments resulting from bending on a load application area of 40 mm x 40 mm, with a load speed of 2400 ± 200 N/s. The measured compressive strength was f_c = 66.75 (2.75) MPa while the flexural strength $f_{c,fl}$ was 1.55 (0.07) MPa. Also these test were performed at the same time as pull-out tests.

The strands, as mentioned, have a nominal diameter d_p = 15.7 mm and area A_p = 150 mm^2. They were cut from prestessing strand coils. The mechanical properties declared on the manufacturer's datasheet, measured according to prEN10138 [37], are yield stress $f_{p0.1k}$ = 1640 MPa, ultimate stress f_{pk} = 1860 MPa, Young's modulus E_p = 195 GPa. Before use, the strands were stored in the laboratory, and protected against corrosion. Furthermore, their surface was not treated in any way but left as it was.

2.3. Experimental setup

Pull-out tests were carried out using an Instron 8862 universal electromechanical testing machine with a purpose-built contrast steel frame. The strand was gripped using a cylindrical prestressing anchor block (barrel) and the corresponding spindle (wedge). The block was connected via a ring attached to the machine actuator (Fig. 4). An axial spherical plane bearing was interposed between the anchorage and the ring, allowing rotation and tilting about the specimen axis to avoid secondary torsional and bending stresses at the strand/grout interface. It is well known that in pull-out tests, the strand tends to rotate due to its geometry [10,11]. Therefore, when the specimen is restrained, a torque is generated, which also depends on the torsional stiffness of the free part of the strand. The stiffness depends on the cross-sectional area of the strand but also on its length, which varies during the test. Different torsional stiffnesses result in different torques and, in principle, different bond–slip laws. For this reason, some standards, such as ASTM A1081 [24], in order to always have the same conditions, require that the specimen be allowed to rotate by placing it on a layer of neoprene. Alternatively, anchoring the strand by using a bearing is suggested. The latter solution has been adopted in the present work, using an axial spherical plane bearing.

Displacement measurements between the strand and concrete (slips) were made using a linear variable displacement transducer (LVDT), measurement range ± 15 mm, placed on the free part of the strand and supported by a metal tripod frame (radius 35 mm) connected to the upper concrete surface of the specimen. This permitted reading directly the slip value. Four further LVDTs were placed under the lower steel contrast plate, one on each side, to detect any bending or differential settlement of the plate itself. The load was measured by the load cell of the testing machine.

2.4. Experimental tests

The test was conducted by controlling the displacement of the loaded part of the strand, operating at a speed of 1 mm/min and achieving a maximum slip of 20 mm in approximately 20 min. As will be seen in Section 3, it was not possible to operate in slip control of the free edge of the strand. Some unsuccessful attempts have been made with an LVDT speed of 0.01 mm/min but, after the peak load, the free edge moves in jumps and the machine is not fast enough to control them. In the case of setup rotations reported by the four LVDTs in the very early phase of the load ramp, the test was stopped and the specimen was unloaded and re-positioned to eliminate eccentricities. During the test, both vertical and horizontal rotations of the spherical plane bearing were observed.

3. Discussion of the experimental results

The tests allowed the force F - slip s curve to be plotted for each specimen. Assuming that the stresses on the nominal bond surface $S_p = 4/3\pi d_p l_b$ (i.e., the outer surface of the strand) are essentially constant, dividing the force F by the surface S_p gives the bond stress $\tau = F/S_p$ and the experimental bond - slip $\tau - s$ curve. Fig. 5a shows the calculation for specimen NC-ND-05, chosen as a paradigmatic case.

It can be seen that the curve has a steep upward branch to the peak τ_1 (point A). Then, there is a jump up to point B, followed by a branch of gradual rising up to point C, where another jump occurs. In this phase the curve has a sawtooth shape with gradually increasing jumps. The progress of the slip by jumps is also visible to the naked eye. The force–displacement curve of the actuator $F-u$ (Fig. 5b) shows that the jumps occur with virtually no displacement u of the actuator. This is probably due to the elastic potential energy stored in the strand, which acts like a spring. To limit this effect, the free length of the loaded part of the strand was minimised.

Considering the shape of the jumps, it is as if the strand loses grip and starts to slip. At this point, the load decreases until the grip is restored and the curve begins to rise again. The phenomenon is repeated many times with increasing amplitude. This phenomenon could be due to the Hoyer effect. In fact, as the force F increases, the strand contracts its cross section or changes its geometry by de-twisting and loses adhesion, causing the force F to decrease. At this point, due to the reduction of F, the cross-section expands and the strand regains adhesion. Note that this phenomenon occurs for very large slip values, well beyond the slip s_1 at the first peak τ_1 (point A in Fig. 5a).

This behaviour has been observed experimentally by other authors. Martí-Vargas et al. [19] studied pretensioned strands subjected to an initial state of tension. The slip force curve for an anchorage length of 50 mm had a similar shape to the one observed here and was slightly saw-toothed. Orr et al. [38] also observed a saw-toothed curve similar

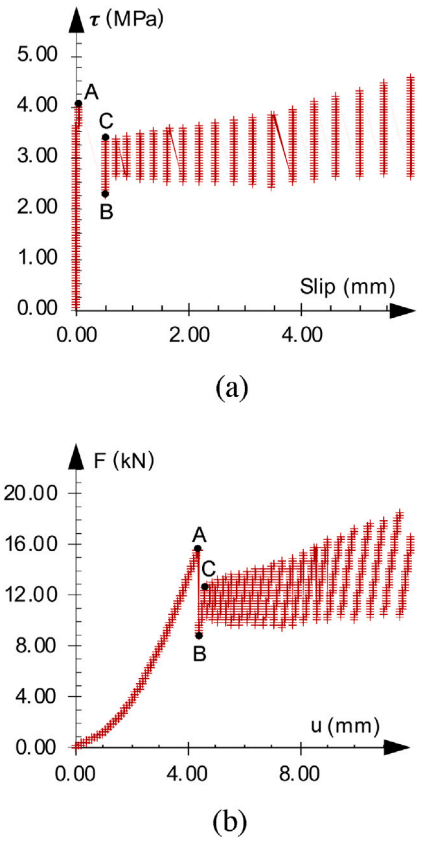

Fig. 5. Experimental results for specimen NC-ND-05: (a) Bond stress-slip $\tau - s$ at the free edge; (b) Force-actuator displacement $F - u$.

in magnitude to those reported here, but only for certain specimen types. All these experimental tests showing jumps were characterised by short anchorage lengths. In fact, with long lengths, the tension in the strand is not constant over the length, so only one part of the strand shows the jump, while the others smooth out its behaviour.

The experimental curves for the six defect-free (NC-ND) specimens are compared in Fig. 6a. Despite the dispersion of the curves, which is typical of bond tests with short bond lengths, very similar behaviour can be observed between the six specimens. Fig. 6b shows a zoom the curves around the first peak. In the case of 25% defects (NC-D25), the curves have the same shape but lower maximum bond strength τ_1 (Fig. 6c, d). Even with 50% defects (NC-D50), the curves retain the same shape but the bond strengths are further reduced (Fig. 6e, f). It can also be observed that after the first peak, the curves tend to flatten as the defect increases.

4. Bond–slip relationship

The experimental curves were used to define the bond–slip relationship. After the first peak τ_1, the experimental data show a jump followed by and an oscillatory trend with a rather variable amplitude between the different samples (Fig. 6). An oscillatory bond–slip law would therefore be rather uncertain. Furthermore, its use, for example in finite element software, would present numerical challenges. For these reasons, it was preferred to fit the envelope of the maxima, average, and minima points rather than interpolate the oscillations of the experimental curve, e.g. with a trigonometric function. A generic maximum point was defined as a point immediately before a jump and a minimum as a point immediately after a jump. The average point was the mean between a minimum and the subsequent maximum.

The law proposed by Guo et al. [15] for post-tensioned strands was initially considered. The law consists of a first linear branch, a second linear descending branch and a third hardening branch defined by a power law. This law has been taken as a starting point in the present work, but some modifications have been made. In particular, a power law was preferred for the first branch because it better represents the experimental curves (Figs. 6b, d, f) and allows for finite transmission lengths [39]. Furthermore, a logistic function was used for the third branch, as it not only better follows the bend shown by the experimental curves (Figs. 6a, c, e), but also has a horizontal asymptote τ_3 for slip values going to infinity, thus avoiding the paradox of the power law of having infinite bond strength.

A schematic drawing of the proposed law, with significant points, is shown in red in Fig. 7. The corresponding equation is:

$$\tau(s) = \begin{cases} \tau_1 \left(\frac{s}{s_1}\right)^{\alpha} & s < s_1 \\ \tau_1 + \left(\frac{\tau_2 - \tau_1}{s_2 - s_1}\right)(s - s_1) & s_1 \le s < s_2 \\ \tau_2 + \frac{\tau_3 - \tau_2}{1 + \left(\frac{s - s_2}{s_0}\right)^{\gamma}} & s \ge s_2 \end{cases} \quad (1)$$

where α and γ are coefficients, whereas stresses τ_1, τ_2, τ_3, and slips s_1, s_2 are shown in Fig. 7. The logistic function was used to interpolate the envelope of the maxima and averages, but it is unsuitable for the minima, which do not have a clear S-shaped trend but are practically constant. In this case, the logistic branch was replaced by a constant branch, giving a bond–slip curve that has the same equation as that proposed by MC2010 [40] for ribbed bars:

$$\tau(s) = \begin{cases} \tau_1 \left(\frac{s}{s_1}\right)^{\alpha} & s < s_1 \\ \tau_1 + \left(\frac{\tau_2 - \tau_1}{s_2 - s_1}\right)(s - s_1) & s_1 \le s < s_2 \\ \tau_2 & s \ge s_2 \end{cases} \quad (2)$$

In Fig. 7, the equation is displayed in blue. The parameters in this equation are identical to those in Eq. (1), with $\tau_3 = \tau_2$.

The two equations were used to fit the experimental curves using the minimum least squares method. The fitting was carried out individually for each experimental curve. Fig. 8 shows the results for specimen NC-ND-01. In particular, Fig. 8a shows the three fitting curves (maximum, average, and minimum) whereas Fig. 8b better shows a detail of the first two branches. Fig. 8a also displays the experimental points of maxima, average, and minima.

The coefficients computed for the first branch and the corresponding R^2 values are collected in Table 1 for all the specimens.

The same table shows the mean value of the coefficients and the corresponding coefficient of variation CV. For specimens without defects, the mean values are $s_1 = 0.026$ mm and $\alpha = 0.128$. The coefficients proposed by Model Code 2010 [40] and confirmed by Model Code 2020 [41] for ribbed bars and "good bond conditions" are $s_1 = 1.0$ mm and $\alpha = 0.4$. For the tested strands, the s_1 values are one-fortieth than Model Code 2010 [40] and the α power is about one-third.

The experimentally measured defect-free τ_1 values were compared with those reported in the literature for short anchors and corrugated steel ducts. In particular, Fig. 9 shows the values of τ_1 as a function of the compressive strength of the grout f_c. It can be seen that the measured values of τ_1, represented by circles, are in agreement with those reported by Guo et al. [31]. On the contrary, the values given by Model Code [40,41] for ribbed bars and "good bond conditions" or "other bond conditions" are both very large.

The results of the fit to the third branch are reported in Table 2. The table shows the parameters for the curve of maxima, averages, and minima. Recall that while the first two were represented with the logistic curve, the curve of minima was represented with a constant. Again, the coefficient of determination R^2 is given, which is generally greater than 0.9. The same table shows also the mean value and the coefficient of variation CV of the different parameters.

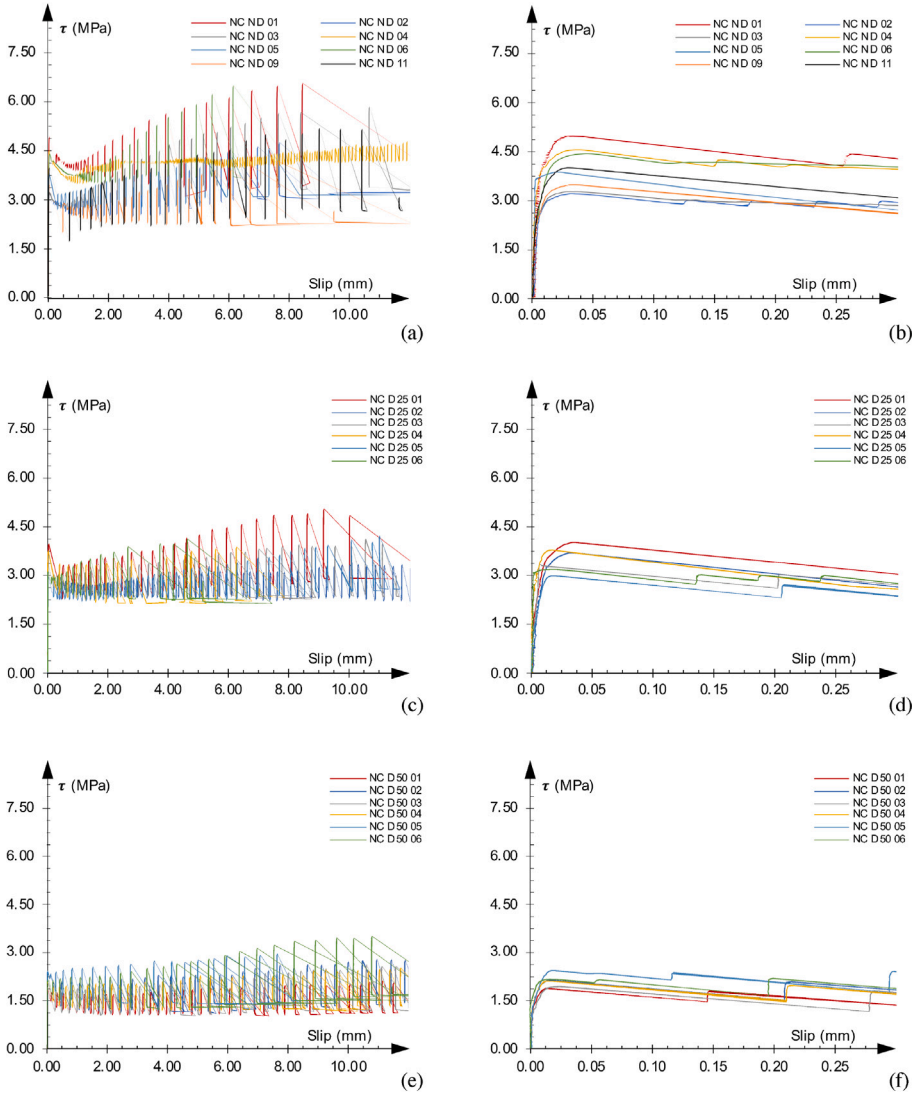

Fig. 6. Experimental bond–slip curves: (a) Specimens NC-ND; (b) Zoom of the initial part of the curves for specimens NC-ND; (c) Specimens NC-D25; (d) Zoom of the initial part of the curves for specimens NC-D25; (e) Specimens NC-D50; (f) Zoom of the initial part of the curves for specimens NC-D50.

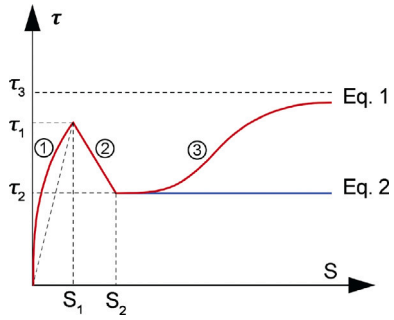

Fig. 7. Schematic drawing of the proposed bond–slip $\tau - s$ relationships.

The mean values of the parameters, which are reported in Tables 1, 2, allow the proposed bond–slip law to be defined.

Fig. 10a shows the proposed bond–slip laws (max, average, and min) for the no-defect case (NC-ND). The laws proposed by Guo et al. [31] and the Model Code 2010 [40], both for "good bond conditions" and "all other conditions", are represented in the same figure. For better comparison of the shapes of the curves, the dimensionless values τ/τ_1 are shown in Fig. 10b. The proposed laws and the one published by Guo et al. [31] are similar, whereas the ones given in the Model Code 2010 [40] are rather different. Obviously, the latter was not designed for prestress strands but for ribbed bars.

For problems where it is prudent to underestimate the bond stresses, and consequently to overestimate the transmission length, it is recommended to use the envelope of minima (min curve in Fig. 10). On the other hand, if it is necessary to overestimate the bond stresses, it is better to use the envelope of maxima (max curve). In other cases, such as FEM modelling, the mean value envelope may be preferable (average curve).

It should also be noted in Fig. 8b that for slip values less than $\approx$ 1.5 mm, the logistic function is practically horizontal and could be replaced by a constant value τ_2, i.e. the curve of minima (Eq. (2)). For most problems, the curve of minima would be sufficient, with the advantage that it has the same expression as the Model Code 2010 [40] curve, which is implemented in many structural analysis software. For ease of reading, the parameters of the curve of minima are summarised in the Table 3.

5. Bond–slip relationship in case of defects

The fitting procedure was also applied to the experimental curves with defects. Table 1 shows the parameters obtained for the first

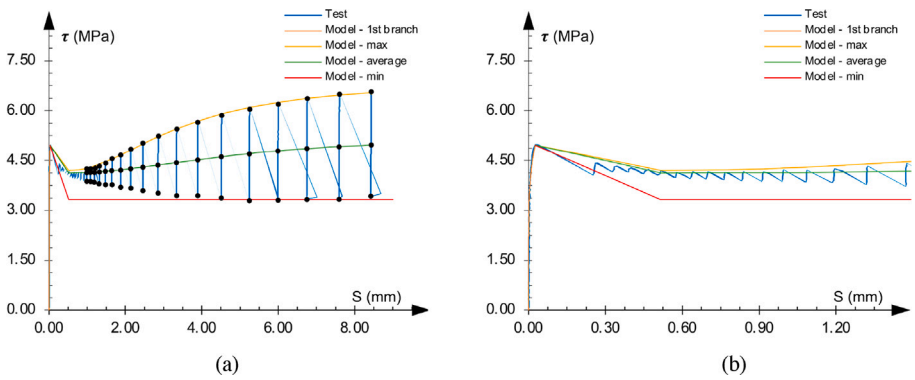

Fig. 8. Fitting of bond–slip curve using the proposed relationship (specimen NC-ND-01): (a) Comparison between test and proposed relationship ; (b) Zoom of the initial part of the curves.

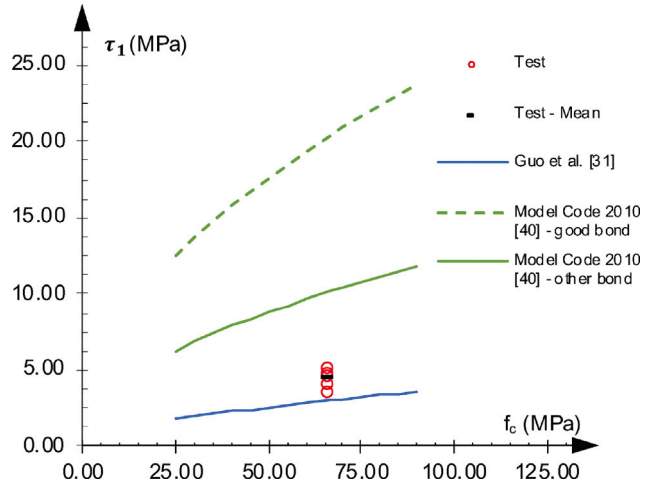

Fig. 9. Bond strength τ_1 as a function of compressive strength of grout f_c: comparison between tests and values reported in the literature.

Table 1
Best fitting of the first branch of bond–slip curves.

Specimen		τ_1 (MPa)	s_1 (mm)	α (–)	R^2 (–)
NC-ND	01	4.96	0.026	0.174	0.94
	02	3.20	0.026	0.136	0.83
	03	3.25	0.024	0.136	0.95
	04	4.53	0.029	0.121	0.93
	05	3.88	0.016	0.036	0.68
	06	4.42	0.038	0.173	0.84
	Mean	4.04	0.026	0.128	0.86
	CV	0.18	0.27	0.40	0.12
NC-D25	01	4.01	0.031	0.220	0.90
	02	3.68	0.027	0.257	0.87
	03	1.93	0.016	0.232	0.96
	04	3.77	0.013	0.224	0.96
	05	2.97	0.015	0.418	0.98
	06	3.17	0.010	0.021	0.46
	Mean	3.26	0.019	0.226	0.85
	CV	0.23	0.45	0.56	0.23
NC-D50	01	1.87	0.011	0.203	0.99
	02	2.13	0.013	0.211	0.98
	03	1.93	0.016	0.232	0.96
	04	2.10	0.011	0.229	0.99
	05	2.43	0.015	0.268	1.00
	06	2.15	0.011	0.172	0.73
	Mean	2.12	0.013	0.219	0.94
	CV	0.09	0.17	0.15	0.11

branch, while Table 2 summarises the parameters for the second and third branches.

The three proposed bond–slip laws (max, average, and min) were compared for the case $\delta = 0\%$, i.e. no defect, (Fig. 11a), $\delta = 25\%$ (Fig. 11b), and $\delta = 50\%$ (Fig. 11c). It can be seen that, as the defect δ increases, the curves become lower and tend to flatten, i.e. the S becomes a straight line. Again, the curve of minima can be used for most problems. Its parameters are summarised in Table 3 for ease of reading.

In order to study the effect of the defect and to compare it to previous studies, the bond strength τ_1 was plotted in Fig. 12a as a function of the parameter β, defined by Guo et al. [31] as the angle at the centre of the arc subtending the defect. It can be seen that the dispersion of the experimental points is important. The same figure shows the experimental points measured by Guo et al. [31] for a strand with a diameter 15.1 mm, duct diameter 55 mm, and bonded length $l_b = 500$ mm (the compressive strength of the grout is not available). Compared to the present tests, their bond stresses without defects are slightly lower and the stresses drop more in the presence of defects. Furthermore, their dispersion of results is significantly lower. This could be due to the longer anchor lengths used by Guo et al. [31], which are less sensitive to injection defects and irregularities. To better compare the results, the average bond values τ_1 were calculated and divided by the corresponding average value without defects $\tau_{1,ND}$, such that the points without defects starts at one for both cases (Fig. 12b). In the same figure, the hidden line represents the variation of the relative bonded area with β, i.e. the ratio between the bonded area with and without defect. It can be observed that the bonded area decreases linearly with β, and the reduction in τ_1 with β is almost linear, taking into account the experimental uncertainties. On the contrary, the experimental values measured by Guo et al. [31] show a reduction that is more than linear, as also observed by the authors. This may be due to the fact that their defect does not expose the strand surface, but only affects part of the grout. However, this difference could also be partly explained by the statistical scatter of the proposed experimental results.

In the present case, experimental results suggest that the bond strength τ_1 in the presence of a defect δ can be computed as

$$\tau_1 = (1 - \delta)\tau_{1,ND} \tag{3}$$

where δ is the defect (in our case 0.25 or 0.5), and $\tau_{1,ND}$ is the bond strength without defect. Fig. 13 shows the variation of the various parameters of the proposed bond–slip law as a function of defect δ. For the bond stresses a general decrease with the defect can be observed (Fig. 13a). On the other hand, the slip increases (Fig. 13b). This phenomenon is more evident for slip s_0, which determines the flattening of the curve. However, the dispersion of the parameters and the small number of experimental points suggest caution in defining an equation linking the parameters to the defect δ.

Table 2
Best fitting of the second and third branches of bond–slip curves.

Specimen		Max						Average					Min
		s_2 (mm)	τ_2 (MPa)	τ_3 (MPa)	s_0 (mm)	γ (–)	R^2 (–)	τ_2 (MPa)	τ_3 (MPa)	s_0 (mm)	γ (–)	R^2 (–)	τ_2 (MPa)
NC-ND	01	0.52	4.20	6.91	3.04	1.94	1.00	4.12	5.27	4.61	1.98	0.99	4.05
	02	0.49	2.91	6.10	5.75	1.64	0.99	2.73	4.64	5.66	2.12	0.99	2.54
	03	0.43	2.86	6.86	4.09	1.33	1.00	2.79	4.87	3.02	1.70	1.00	2.71
	04	0.52	3.77	5.07	4.60	1.30	0.86	3.75	4.80	4.50	1.24	0.86	3.72
	05	0.31	3.25	5.21	4.54	1.58	0.99	2.98	4.39	5.42	1.72	0.98	2.72
	06	0.73	3.79	7.82	3.72	1.99	1.00	3.79	5.61	3.58	2.44	0.99	3.79
	Mean	0.50	3.46	6.33	4.29	1.63	0.97	3.36	4.93	4.46	1.87	0.97	3.25
	CV	27.62	15.58	16.93	21.39	17.96	5.72	17.75	8.93	22.90	21.97	5.73	20.51
NC-D25	01	0.52	3.34	5.65	5.25	1.87	0.98	2.99	4.08	4.93	2.91	0.99	2.64
	02	0.49	2.79	3.55	6.18	1.67	0.97	2.58	2.84	5.47	1.89	0.68	2.38
	03	0.20	3.08	4.57	6.81	1.60	0.99	2.79	3.37	6.75	2.14	0.98	2.50
	04	0.39	3.37	5.16	8.58	2.10	0.97	2.80	3.15	4.56	4.46	0.93	2.23
	05	0.33	2.71	4.57	7.02	1.90	0.98	2.50	4.35	12.71	1.69	0.97	2.28
	06	0.14	3.02	4.22	1.39	1.70	0.99	2.81	3.23	1.78	1.89	0.96	2.60
	Mean	0.39	3.05	4.62	6.77	1.80	0.98	2.74	3.50	4.70	2.11	0.92	2.44
	CV	33.31	8.93	15.82	18.14	10.26	1.01	6.43	16.64	20.47	22.66	12.89	6.90
NC-D50	01	0.33	1.80	2.07	5.56	4.35	0.91	1.43	1.73	9.59	2.69	0.76	1.07
	02	0.21	2.10	2.92	6.55	2.59	0.93	1.68	2.24	8.23	3.25	0.95	1.25
	03	0.28	1.87	3.06	8.56	1.85	0.98	1.52	1.93	6.37	4.79	0.99	1.18
	04	0.41	1.99	2.51	5.05	1.55	0.89	1.63	1.80	4.26	3.61	0.89	1.27
	05	0.30	2.42	3.56	8.10	1.00	0.94	2.05	2.31	6.46	3.65	0.91	1.68
	06	0.43	2.25	4.02	6.45	2.19	1.00	1.80	2.79	6.77	2.71	0.99	1.35
	Mean	0.33	2.07	3.02	6.71	1.83	0.94	1.69	2.13	6.95	3.45	0.92	1.30
	CV	25.59	11.40	23.25	20.57	33.07	4.32	12.99	18.60	26.09	22.53	9.46	16.06

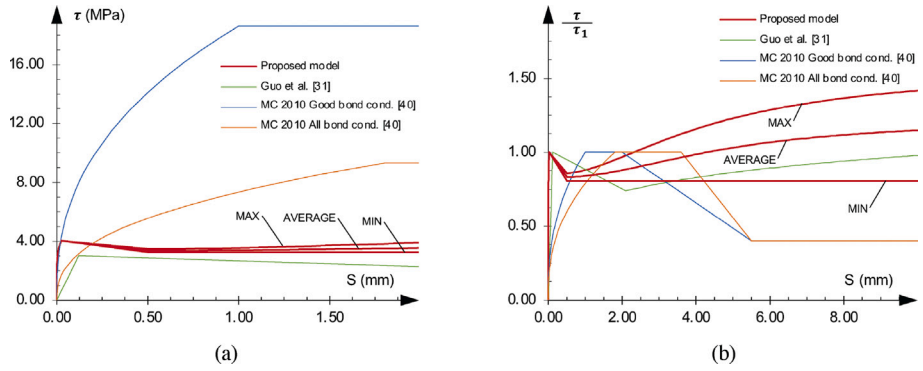

Fig. 10. Comparison of bond–slip relationships: (a) Bond–slip relationships around the first peak; (b) Dimensionless bond–slip relationships for the entire slip range.

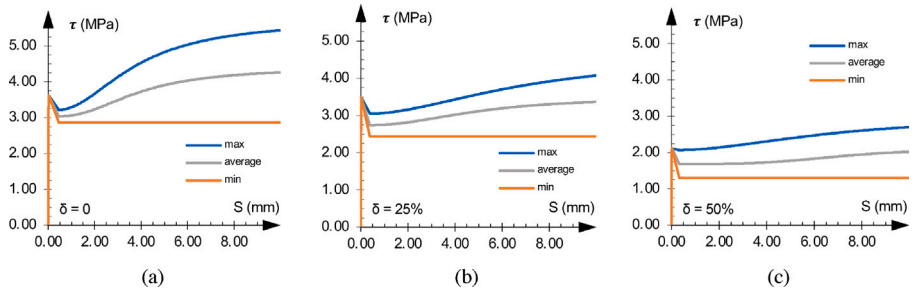

Fig. 11. Comparison of proposed bond–slip relationships: (a) No defect (NC-ND); (b) Defect 25% (NC-D25); (c) Defect 50% (NC-D50).

6. Conclusions

This paper describes a campaign of unstressed pull-out tests to investigate the bond of pre-tension strands with and without grout injection defects. After a thorough discussion of the decisions made in designing the test set-up, the paper describes the test results. In particular, all the experimental curves show an initial curvilinear branch, a jump descent and then, at high slip values, a gradually increasing oscillatory trend. The experimental results were used to calibrate a specific bond–slip law. Instead of simulating the oscillatory trend, three curves were proposed for the envelope of maxima, average, and minima. In the case of the envelope of minima, the curve has the same shape as that proposed for ribbed bars by Model Code 2010 [40]. It consists of a first branch described by a power law, a linear descending branch and

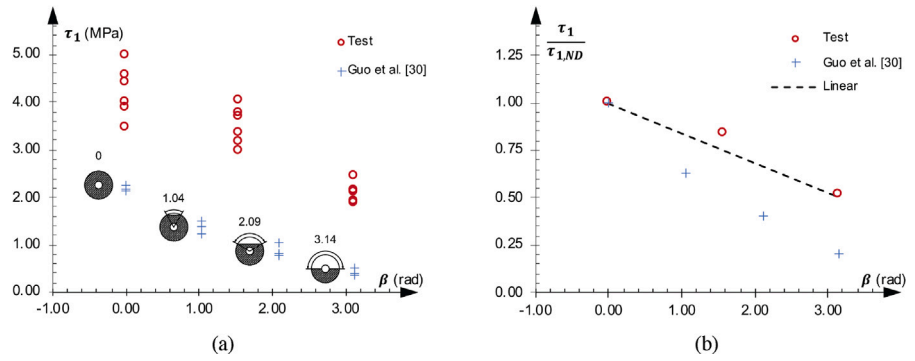

Fig. 12. (a) Maximum bond strength τ_1 as a function of defect angle β; (b) Dimensionless average bond strength $\tau_1/\tau_{1,ND}$ as a function of defect angle β.

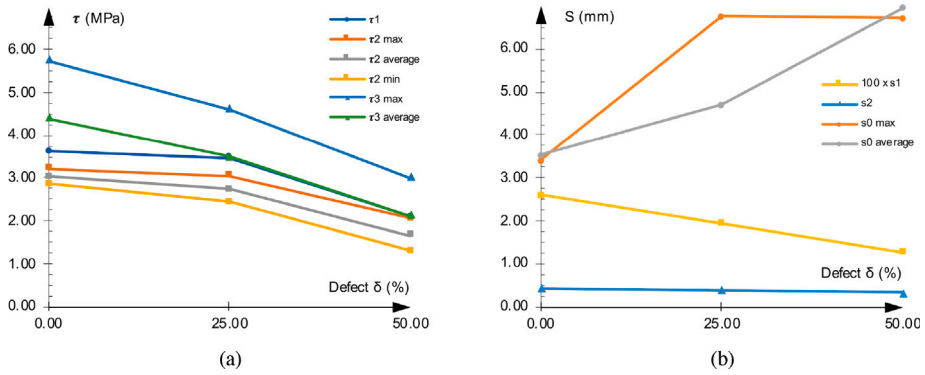

Fig. 13. Parameters of bond–slip law: (a) Bond parameters as a function of defect extension δ; (b) Slip parameters as a function of defect extension δ. Note that for representation problems, the value $100 \times s_1$ is shown.

Table 3
Parameters of the proposed bond–slip law (Eq. (2)) for different defects δ. The meaning of the parameters is shown in Fig. 7.

δ	τ_1 (MPa)	s_1 (mm)	α (–)	s_2 (mm)	τ_2 (MPa)
0%	4.04	0.026	0.128	0.50	3.25
25%	3.26	0.019	0.226	0.39	2.44
50%	2.12	0.013	0.219	0.33	1.30

a third constant branch. For the envelope of the maxima or average values, the third constant branch is replaced by a logistic function, which better follows the increasing S-shaped trend. The experimental results show that:

- For small slips, the bond–slip law for post-tensioning strands has the same form as that proposed by Model Code 2010 [40] for ribbed bars, but with very different parameters (Table 3).
- The presence of defects reduces the surface area of the strand in contact with the grout. Consequently, the bond strength τ_1 is reduced approximately by the ratio of the area in contact with the defect to the area without the defect.
- As defects increase, bond stresses decrease while slips increase, with a flattening of the third branch of the curve.

It is clear that these observations refer to the ideal case studied here. In practice, the duct usually contains several strands, not all of which are wrapped with the same thickness of mortar. In addition, if the duct is curved, the strands are only on one side and not in the centre of the duct. Finally, the duct and the strand are often subject to corrosion [42,43]. The problem is very complex, so simplifying assumptions have been made to begin to understand the basic mechanisms. Future studies will need to include the aspects that have not been considered here, as well as the important issue of strand corrosion.

CRediT authorship contribution statement

Daniele Ferretti: Writing – review & editing, Writing – original draft, Supervision, Software, Methodology, Investigation, Formal analysis, Conceptualization. **Federico Pagliari:** Visualization, Investigation, Formal analysis, Data curation. **Beatrice Belletti:** Supervision, Project administration, Methodology, Funding acquisition, Conceptualization.

Declaration of competing interest

The authors declare the following financial interests/personal relationships which may be considered as potential competing interests: Beatrice Belletti reports financial support was provided by RELUIS. The other authors declare that they have no known competing financial interests or personal relationships that could have appeared to influence the work reported in this paper.

Data availability

Data will be made available on request.

Acknowledgements

The study presented was carried out as part of the Agreement between Consiglio Superiore dei Lavori Pubblici, Italy and ReLUIS, Italy according to DM 578/2020 and DM 240/2022.

References

[1] R. Tepfers, Z. Achillides, A. Azizinamini, G. Balázs, A.B. van Vliet, J. Cabrera, J. Cairns, E. Cosenza, J. den Uijl, R. Eligehausen, B. Engström, L. Erdélyi, P. Gambarova, J. Jirsa, S. Lane, R. Leon, J. Magnusson, U. Mayer, S. McCabe, C. Modena, J. Modniks, T.J. Mottram, K. Noghabai, K. Otsuka, J. Ozbolt, S.J. Pantazopoulou, K. Pilakoutas, G. Plizzari, R. Realfonzo, J. Rodriguez, G.P.

Rosati, G. Russo, S. Russo, H. Shima, C. Schumm, L. Taerwe, V. Tamuzs, T. Ueda, L. Vandewalle, L. Vintzileou, fib Bulletin 10. Bond of Reinforcement in Concrete, fib. The International Federation for Structural Concrete, 2000, http://dx.doi.org/10.35789/fib.BULL.0010.

[2] G.A. Plizzari, J. Cairns, G. Metelli, M.A. Aiello, J. Bošnjak, G. Centonze, F. Ceroni, O.C. Choi, H. Choi, A. Conforti, D. Coronelli, D. Darwin, R. Eligehausen, N. Fabris, F. Faleschini, A.P. Fantilli, I. Fernandez, P.G. Gambarova, G. Haikal, J. Hegger, J. Hofmann, K.Y. Kim, H. Lakhani, M. Leone, A. Lepage, F.L. Monte, K. Lundgren, E. Marchina, K.G. Megalooikonomou, M. Micallef, G. Muciaccia, S.J. Pantazopoulou, M.R. Pecce, C. Pellegrino, J.A. Ramirez, Z. Rinaldi, J. Schoening, A. Sharma, J. Silva, M. Tahershamsi, S.P. Tastani, F. Tondolo, R.L. Vollum, S. Yasso, K. Zandi, M.A. Zanini, fib Bulletin 106. Advances on Bond in Concrete, fib. The International Federation for Structural Concrete, 2022, http://dx.doi.org/10.35789/fib.BULL.0106.

[3] L. Dai, Y. Chen, L. Wang, Y. Ma, Secondary anchorage and residual prestressing force in locally corroded PT beams after strand fracture, Constr. Build. Mater. 275 (2021) 122137, http://dx.doi.org/10.1016/j.conbuildmat.2020.122137.

[4] O. Asp, J. Tulonen, L. Kuusisto, A. Laaksonen, Bond and re-anchoring tests of post-tensioned steel tendon in case of strand failure inside cement grouting with voids, Struct. Concr. 22 (4) (2021) 2373–2390, http://dx.doi.org/10.1002/suco.202000351.

[5] D. Yaohua, G. Morcous, Z.J. Ma, Strand bond stress–slip relationship for prestressed concrete members at prestress release, Mater. Struct. 49 (3) (2015) 889–903, http://dx.doi.org/10.1617/s11527-015-0546-1.

[6] L. Dai, W. Xu, L. Wang, S. Yi, W. Chen, Secondary transfer length and residual prestress of fractured strand in post-tensioned concrete beams, Front. Struct. Civ. Eng. 16 (3) (2022) 388–400, http://dx.doi.org/10.1007/s11709-022-0809-1.

[7] T. Mostafa, P. Zia, Development length of prestressing strands, PCI J. 22 (5) (1977) 54–65, http://dx.doi.org/10.15554/pcij.09011977.54.65.

[8] J.R. Janney, Nature of bond in pre-tensioned prestressed concrete, ACI J. Proc. 50 (5) (1954) 717–736, http://dx.doi.org/10.14359/11790.

[9] H.H. Abrishami, D. Mitchell, Bond characteristics of pretensioned strand, ACI Mater. J. 90 (3) (1993) 228–235, http://dx.doi.org/10.14359/3785.

[10] J. Yi, L. Wang, R.W. Floyd, J. Zhang, Rotation-affected bond strength model between steel strand and concrete, Eng. Struct. 204 (2020) 110060, http://dx.doi.org/10.1016/j.engstruct.2019.110060.

[11] L. Wang, P. Yuan, G. Xu, Y. Han, Quantification of non-uniform mechanical interlock and rotation in modelling bond-slip between strand and concrete, Structures 37 (2022) 403–410, http://dx.doi.org/10.1016/j.istruc.2022.01.024.

[12] E. Hoyer, E. Friedrich, Beitrag zur frage der haftspannung in eisenbetonbauteilen, Beton Eisen 50 (9) (1939) 717–736.

[13] V. Briere, K.A. Harries, J. Kasan, C. Hager, Dilation behavior of seven-wire prestressing strand – The Hoyer effect, Constr. Build. Mater. 40 (2013) 650–658, http://dx.doi.org/10.1016/j.conbuildmat.2012.11.064.

[14] H. Kobrosli, O. Baalbaki, A. Jahami, Z.A. Saleh, J. Khatib, M. Serkan Kırgız, A. Gustavo de Sousa Galdino, Influence of various design parameters of the grouted duct on mono-strand bond behavior in post tensioned members, J. Mater. Res. Technol. 17 (2022) 1232–1245, http://dx.doi.org/10.1016/j.jmrt.2022.01.034.

[15] R. Guo, Z. Zhen, S. Zhao, C. Li, Effects of grouting defects in a duct on the bonding of prestressing strands, KSCE J. Civ. Eng. 24 (4) (2020) 1268–1275, http://dx.doi.org/10.1007/s12205-020-0892-6.

[16] R.W. Keuning, M.A. Sozen, C.P. Siess, A Study of Anchorage Bond in Prestressed Concrete, Structural Research Series No. 251, University of Illinois, Urbana-Champaign, IL, 1962.

[17] T.E. Cousins, M.H. Badeaux, S. Moustafa, Proposed test for determining bond characteristics of prestressing strand, PCI J. 37 (1) (1992) 66–73, http://dx.doi.org/10.15554/pcij.01011992.66.73.

[18] D.R. Rose, B.W. Russell, Investigation of standardized tests to measure the bond performance of prestressing strand, PCI J. 42 (4) (1997) 56–80, http://dx.doi.org/10.15554/pcij.07011997.56.80.

[19] J. Martí-Vargas, W. Hale, E. García-Taengua, P. Serna, Slip distribution model along the anchorage length of prestressing strands, Eng. Struct. 59 (2014) 674–685, http://dx.doi.org/10.1016/j.engstruct.2013.11.032.

[20] J. den Uijl, Bond modelling of prestressing strand, in: SP-180: Bond and Development of Reinforcement - a Tribute To Dr. Peter Gergely, American Concrete Institute, 1998, http://dx.doi.org/10.14359/5876.

[21] J. den Uijl, Bond and splitting action of prestressing strand, in: Proceedings, Bond in Concrete, Riga, Latvia, October 15-17-1992, CEB, 1992, p. 2.

[22] C.N. Dang, R.W. Floyd, C.D. Murray, W.M. Hale, J.R. Martí-Vargas, Bond stress-slip model for 0.6 in. (15.2 mm) diameter strand, ACI Struct. J. 112 (5) (2015) http://dx.doi.org/10.14359/51687750.

[23] A. Pozolo, B. Andrawes, Analytical prediction of transfer length in prestressed self-consolidating concrete girders using pull-out test results, Constr. Build. Mater. 25 (2) (2011) 1026–1036, http://dx.doi.org/10.1016/j.conbuildmat.2010.06.076.

[24] ASTM A1081/A1081M-21, Standard Test Method for Evaluating Bond of Seven-Wire Steel Prestressing Strand, ASTM International, 2021.

[25] C.N. Dang, C.D. Murray, R.W. Floyd, W.M. Hale, J. Martí-Vargas, Analysis of bond stress distribution for prestressing strand by standard test for strand bond, Eng. Struct. 72 (2014) 152–159, http://dx.doi.org/10.1016/j.engstruct.2014.04.040.

[26] P. Mohandoss, R.G. Pillai, R. Gettu, Determining bond strength of seven-wire strands in prestressed concrete, Structures 33 (2021) 2413–2423, http://dx.doi.org/10.1016/j.istruc.2021.06.004.

[27] X. Xiong, L. He, Z. Zhou, Q. Xiao, The bond-slip constitutive model of retard-bonded prestressing steel strand, Constr. Build. Mater. 365 (2023) 129995, http://dx.doi.org/10.1016/j.conbuildmat.2022.129995.

[28] H. Kobrosli, O. Baalbaki, A. Jahami, Z.A. Saleh, J. Khatib, M. Sonebi, Effect of duct type, size, and embedment on bond behavior of post-tensioned mono-strand concrete members, Mater. Today: Proc. 58 (2022) 1205–1210, http://dx.doi.org/10.1016/j.matpr.2022.01.422.

[29] T. Lüthi, J.R. Diephuis, J.J.I. A., J.E. Breen, M.E. Kreger, Effects of duct types and emulsifiable oils on bond and friction losses in posttensioned concrete, J. Bridge Eng. 13 (1) (2008) 100–109, http://dx.doi.org/10.1061/(asce)1084-0702(2008)13:1(100).

[30] J. Laco, V. Borzovič, Experimental investigation of prestressing strand bond on behavior of concrete members, ACI Struct. J. 114 (1) (2016) http://dx.doi.org/10.14359/51689146.

[31] T. Guo, J. Yang, W. Wang, C. Li, Experimental investigation on connection performance of fully-grouted sleeve connectors with various grouting defects, Constr. Build. Mater. 327 (2022) 126981, http://dx.doi.org/10.1016/j.conbuildmat.2022.126981.

[32] L. Wang, P. Yuan, X. Zhang, Y. Dong, Y. Ma, J. Zhang, Bond behavior between multi-strand tendons and surrounding grout: Interface equivalent modeling method, Constr. Build. Mater. 226 (2019) 61–71, http://dx.doi.org/10.1016/j.conbuildmat.2019.07.242.

[33] T. Luthi, J. Diephuis, J. Icaza, J. Breen, M. Kreger, Factors affecting bond and friction losses in multi-strand post-tensioning tendons including the effects of emulsifiable oils, Tech. rep., Center for Transportation Research, The University of Texas at Austin, 2005.

[34] EN 12390-3:2009, Testing Hardened Concrete - Part 3: Compressive Strength of Test Specimens, European Committee for Standardization, 2009.

[35] EN 12390-6:2010, Testing Hardened Concrete - Part 6: Tensile Splitting Strength of Test Specimens, European Committee for Standardization, 2009.

[36] EN 196-1:2016, Methods of Testing Cement - Part 1: Determination of Strength, European Committee for Standardization, 2015.

[37] prEN 10138-3:2005, Prestressing Steel - Part 3: Strand, European Committee for Standardization, 2005.

[38] J. Orr, A. Darby, T. Ibell, N. Thoday, P. Valerio, Anchorage and residual bond characteristics of 7-wire strand, Eng. Struct. 138 (2017) 1–16, http://dx.doi.org/10.1016/j.engstruct.2017.01.061.

[39] G.L. Balazs, Transfer control of prestressing strands, PCI J. 37 (6) (1992) 60–71, http://dx.doi.org/10.15554/pcij.11011992.60.71.

[40] fib, Model Code for Concrete Structures 2010, Wiley-VCH Verlag GmbH, 2013.

[41] fib, Model Code for Concrete Structures 2020, final draft, 2023.

[42] S. Haefliger, W. Kaufmann, Corroded tension chord model: Load-deformation behavior of structures with locally corroded reinforcement, Struct. Concr. 23 (1) (2022) 104–120, http://dx.doi.org/10.1002/suco.202100165.

[43] L. Wang, X. Zhang, J. Zhang, Y. Ma, Y. Xiang, Y. Liu, Effect of insufficient grouting and strand corrosion on flexural behavior of PC beams, Constr. Build. Mater. 53 (2014) 213–224, http://dx.doi.org/10.1016/j.conbuildmat.2013.11.069.